

# On the Monotonic and Cyclic Behavior of an Al-Mg-Zn-Cu-Si Compositionally Complex Alloy

Seyed Vahid Sajadifar,\* Jörg Baumgartner, Marcel Krochmal, Andreas Maciolek, Marcus Klein, Moritz Rößer, Markus Graß, Hannes Fröck, Martin Fehlbier, Olaf Kessler, Stefan Böhm, Matthias Oechsner, Tobias Melz, and Thomas Niendorf

In present work, the monotonic and cyclic properties of a novel Al-Mg-Zn-Cu-Si compositionally complex alloy (CCA) are investigated. Microstructural studies reveal that a eutectic phase and fishbone-type structures are embedded in the Al-matrix. The mechanical properties of this CCA obtained under compressive loading are found to be promising. However, low ultimate strength and brittle behavior are seen under tension. The fatigue performance of the alloy in the low-cycle fatigue (LCF) regime is poor. Microstructural features and fracture surface analysis point to the fact that the presence of brittle intermetallic phases and shrinkage defects are responsible for the poor tensile properties and inferior LCF behavior. Homogenization at 460 and 465 °C for 3 h, 6 h, and 24 h results in spheroidization of all coarse precipitates. However, the heat treatment used is unsuitable to enhance the mechanical properties of this CCA.

loading.<sup>[3–5]</sup> Although some of the CCAs are single-phase, many of the investigated CCAs were found to be multiphase materials.<sup>[6,7]</sup> Recently, the mechanical and physical properties of multiphase CCAs were correlated to the different phases being present.<sup>[8–10]</sup> One phase may have higher strength, while the other one may have higher ductility, resulting in intriguing mechanical properties. Non-equiatomic CCAs with extraordinary strength–ductility combination were presented and discussed.<sup>[10]</sup> The alloy design strategy was found to be the key to the fabrication of CCAs with excellent strength–ductility combination. Therefore, based on the results of previous studies, a large number of possibilities to design materials

with superior mechanical properties can be offered by mixing different elements.

In recent years, the requirements for reducing carbon dioxide (CO<sub>2</sub>) emissions have led to the development of lightweight alloys.<sup>[11,12]</sup> Replacing high-density metals with lightweight alloys is one of the fundamental aspects for the development of lightweight components. Among lightweight alloys, aluminum (Al)


## 1. Introduction

A new class of materials, namely compositionally complex alloys (CCAs), was proposed by Cantor et al. and Yeh et al. in 2004.<sup>[1,2]</sup> CCAs are a mixture of multiple principal elements. Due to the unique microstructure of the CCAs, these alloys show extraordinary mechanical properties under both monotonic and cyclic

S. V. Sajadifar, M. Krochmal, T. Niendorf  
Institute of Materials Engineering  
University of Kassel  
Mönchebergstraße 3, 34125 Kassel, Germany  
E-mail: sajjadifar@uni-kassel.de

J. Baumgartner, A. Maciolek, T. Melz  
Fraunhofer Institute for Structural Durability and System Reliability LBF  
Bartningstraße 47, 64289 Darmstadt, Germany

M. Klein, M. Oechsner  
Mechanical Engineering  
Center for Structural Materials, State Materials Testing Institute  
Darmstadt (MPA), Chair and Institute for Materials Technology (Ifw)  
Technical University of Darmstadt  
64283 Darmstadt, Germany

 The ORCID identification number(s) for the author(s) of this article can be found under <https://doi.org/10.1002/adem.202300892>.

© 2023 The Authors. Advanced Engineering Materials published by Wiley-VCH GmbH. This is an open access article under the terms of the Creative Commons Attribution License, which permits use, distribution and reproduction in any medium, provided the original work is properly cited.

DOI: 10.1002/adem.202300892

M. Rößer, M. Fehlbier  
Department for Casting-Technology - GTK  
University of Kassel  
Kurt-Wolters-Str. 3, 34125 Kassel, Germany

M. Graß, S. Böhm  
Department for Cutting and Joining Manufacturing Processes  
University of Kassel  
34125 Kassel, Germany

H. Fröck, O. Kessler  
Chair of Materials Science  
University of Rostock  
Albert-Einstein-Str. 2, 18059 Rostock, Germany

H. Fröck, O. Kessler  
Competence Centre CALOR  
Department of Life, Light and Matter  
University of Rostock  
Albert-Einstein-Str. 25, 18059 Rostock, Germany

alloys show outstanding mechanical behavior making them excellent alternatives for the substitution of high-density metals.<sup>[13,14]</sup> With the addition of various alloying elements to the Al alloys, new compositions with different characteristics were developed.<sup>[15–17]</sup> Thus, different series of Al alloys were established. In contrast, the superior strength-to-weight ratio and acceptable formability of Al alloys have resulted in their utilization in numerous applications.<sup>[13,18,19]</sup> Different heat treatments, forming strategies, and thermomechanical treatments are employed to tailor the mechanical properties of Al alloys for various applications.

CCAs being promising for lightweight applications were classified into two groups according to the elements used.<sup>[20]</sup> 1) The CCAs in the group (1) are designed by choosing only light components, including Al, Mg, Li, Be, Zn, Si, Ti, Sn, and Sc. These CCAs usually have very low density ( $1\text{--}4.5\text{ g cm}^{-3}$ ). 2) The CCAs in the group (2) are developed from pre-existing solid solution CCAs. Basically, some heavy elements, e.g., Hf and Ta, are replaced by light elements, e.g., Ti and Al. In the remainder of the text, the CCAs of group (1) and group (2) are called low-density and lightweight CCAs, respectively. Novel low-density CCAs have been recently studied showing great potential for the development of a new class of materials.<sup>[21–24]</sup> These low-density CCAs were among the alloy families introduced by Miracle and Senkov.<sup>[25]</sup> CALPHAD modeling and die casting were employed to design and fabricate novel low-density CCAs such as  $\text{Al}_{40}\text{Cu}_{15}\text{Cr}_{15}\text{Fe}_{15}\text{Si}_{15}$ ,  $\text{Al}_{65}\text{Cu}_5\text{Cr}_5\text{Si}_{15}\text{Mn}_5\text{Ti}_5$ , and  $\text{Al}_{60}\text{Cu}_{10}\text{Fe}_{10}\text{Cr}_5\text{Mn}_5\text{Ni}_5\text{Mg}_5$ .<sup>[26]</sup> The hardness and density of these CCAs were measured to be in the range of 743 to 916 HV and  $3.7\text{ to }4.6\text{ g cm}^{-3}$ , respectively. The highest hardness values were obtained for  $\text{Al}_{40}\text{Cu}_{15}\text{Cr}_{15}\text{Fe}_{15}\text{Si}_{15}$  and  $\text{Al}_{65}\text{Cu}_5\text{Cr}_5\text{Si}_{15}\text{Mn}_5\text{Ti}_5$  CCAs. Results obtained so far<sup>[22,26]</sup> indicate that low-density CCAs are characterized by an excellent application potential. Furthermore, a gravity permanent mold casting process was utilized to manufacture  $\text{Al}_{80}\text{Mg}_5\text{Sn}_5\text{Zn}_5\text{Ni}_5$ ,  $\text{Al}_{80}\text{Mg}_5\text{Sn}_5\text{Zn}_5\text{Mn}_5$ , and  $\text{Al}_{80}\text{Mg}_5\text{Sn}_5\text{Zn}_5\text{Ti}_5$  alloys.<sup>[27]</sup>  $\text{Al}_{80}\text{Mg}_5\text{Sn}_5\text{Zn}_5\text{Ni}_5$ ,  $\text{Al}_{80}\text{Mg}_5\text{Sn}_5\text{Zn}_5\text{Mn}_5$ , and  $\text{Al}_{80}\text{Mg}_5\text{Sn}_5\text{Zn}_5\text{Ti}_5$  CCAs contained multiphase microstructures with a primary  $\alpha$ -aluminum matrix reinforced with secondary phases. A high ultimate compressive strength of 563 MPa and a considerable compressive fracture strain of 12% were reported for  $\text{Al}_{80}\text{Mg}_5\text{Sn}_5\text{Zn}_5\text{Ti}_5$  and  $\text{Al}_{80}\text{Mg}_5\text{Sn}_5\text{Zn}_5\text{Ni}_5$  CCAs, respectively.<sup>[27]</sup> A series of light alloys with elements of Al, Li, Mg, Ca, Si, and Y were designed, fabricated, and explored elsewhere.<sup>[28]</sup> Upon compression, these CCAs exhibited high specific strength, good ductility, and low Young's modulus in comparison to conventional alloys. Among low-density CCAs, some alloys were designed based on the Al-Mg system.<sup>[21,29]</sup> An Al-Mg-Zn-Cu-Si CCA exhibited excellent mechanical properties under compressive loading.<sup>[21]</sup> The microstructure of this CCA was multiphased, consisting of a matrix rich in Al and dendritic structures rich in Mg, Cu, Zn, and Si.

Most published studies on low-density CCAs focus only on the hardness and compression behavior of as-cast alloys.<sup>[26,27]</sup> However, also the tensile properties and fatigue performance of Al-based CCAs should comprehensively be addressed. Since many components are exposed to cyclic loading, the fatigue properties of Al-Mg-Zn-Cu-Si CCA should also be explored comprehensively. Thus, the present study aims to investigate the monotonic tensile and cyclic behavior of the novel Al-13Mg-1.1Zn-0.9Cu-0.6Si (Al-11.5Mg-2.6Zn-2.1Cu-0.6Si in wt%) CCA

for the very first time. In previous studies on low-density CCAs, an Al-11.5Mg-2.6Zn-2.1Cu-0.6Si CCA showed a compression behavior that pointed at its potential use as material in high stressed light-weight constructions.<sup>[21,29]</sup> A pronounced work hardening indicating interactions between dislocations and different phases was evident for this CCA. Therefore, Al-Mg-Zn-Cu-Si CCAs deserve more attention. To unravel the performance under monotonic and cyclic loadings, their mechanical properties have to be comprehensively investigated. In present work, the microstructure of the as-cast condition is analyzed using different techniques. Tensile experiments and low-cycle fatigue (LCF) tests under strain control ( $R = -1$ ) are carried out on the as-cast condition to assess the mechanical properties of the alloy in various loading regimes. Fracture analysis is also reported to reveal the origins of crack initiation. Besides, homogenization was carried out to reveal the effect of heat treatment on the microstructure and mechanical properties of the CCA in focus. Results obtained in present work can guide the future path for the development of low-density CCAs based on the Al-Mg system.

## 2. Experimental Section

To produce the Al-13Mg-1.1Zn-0.9Cu-0.6Si CCA, a mixture of pure aluminum, high-purity alloying elements (Cu, Si, Zn), and an AZ91HP magnesium alloy was melted in a laboratory melting furnace (Nabertherm GmbH, Lilienthal, Germany) using a clay-graphite crucible and cast into a copper mold. The mold temperature was  $100\text{ }^\circ\text{C}$ ; the casting temperature was  $750\text{ }^\circ\text{C}$ . After solidification and removal, the castings were cooled in the air at  $20\text{ }^\circ\text{C}$ . The optical emission spectroscopy (OES) technique was used for the determination of the chemical composition in weight%, as shown in **Table 1**. The Fe content arose from impurities in the AZ91HP magnesium alloy.

Specimens for tensile testing with gauge section dimensions of  $8 \times 3 \times 1.5\text{ mm}^3$  and compression cylinders with a diameter of 6 mm and a height of 10 mm were cut from the as-cast material using electrical-discharge machining (EDM). Specimens were mechanically ground down to 2,500 grit by SiC grinding papers before testing. Tensile and compression experiments were conducted at room temperature employing an MTS criterion tensile testing machine under a crosshead speed of  $2\text{ mm min}^{-1}$ . Three tensile and compression experiments per condition were performed. An MTS miniature extensometer with a gauge length of 5 mm was used to measure the strains during tensile testing. Tensile and compression data were analyzed using the “LabMaster” software.

Vickers hardness tests were carried out on the specimens applying 4.9 N and 15 s indentation duration. Three hardness measurements per condition were conducted. Average values are provided in the present article. Nanoindentation measurements were performed utilizing an Anton Paar NHT<sup>3</sup> tester

**Table 1.** Chemical composition of the Al-13Mg-1.1Zn-0.9Cu-0.6Si alloy used in the present study given in weight%.

Element	Al	Mg	Zn	Cu	Si	Fe
Content [wt%]	82.80	11.47	2.56	2.11	0.55	0.34

(Anton Paar GmbH, Graz, Austria). A Berkovich diamond indenter was used. Maximum force, loading, and unloading rates were 1 mN and 2.00 mN min<sup>-1</sup>, respectively. The approach and retract speeds were selected as 2 μm min<sup>-1</sup>.

For the microstructural studies and nanoindentation measurements, specimens were ground down to 4,000 grit via SiC grinding papers. Then, they were mechanically polished using a colloidal silica suspension. Optical microscopy (OM) was employed to analyze the microstructure. A scanning electron microscope (SEM) equipped with an energy-dispersive spectroscopy (EDS) unit at an accelerating voltage of 20 kV was used to study the microstructure and fracture surfaces. Energy-dispersive (ED) X-Ray diffraction (XRD) measurements were performed employing a system equipped with a Ketek AXAS-M H80 (SDD) detector and a tungsten tube operated at 60 kV and 40 mA. The ED-XRD measurements were carried out at room temperature. The acquisition was conducted at a fixed 2θ° angle with a duration of 8 h. The crystallographic structure of the Al-13Mg-1.1Zn-0.9Cu-0.6Si alloy was refined taking into account a lattice parameter of 0.4083 nm.

The melting behavior was analyzed by differential scanning calorimetry (DSC) using a PerkinElmer Pyris 8500. The sample weight amounted to approximately 45 mg. As a reference, high-purity Al5N5 was applied. Samples were packed in alumina crucibles. The heating process consisted of two stages. Initially, the sample was heated from room temperature to 400 °C at a rate of 1 K s<sup>-1</sup>. Subsequently, it was further heated from 400 to 640 °C at a rate of 0.1 K s<sup>-1</sup>. The obtained heat flow data were normalized by sample mass and heating rate to achieve the excess heat capacity.<sup>[30]</sup>

For the fatigue strength assessment, six specimens were machined by EDM out of the cast material. After EDM, the specimens were polished carefully by hand to remove the EDM affected surface. The global length of the specimens was  $l = 50$  mm, the width  $w = 8$  mm, and the thickness  $t = 2$  mm. In the gauge section the width was reduced to 3.4 mm over a length of 10 mm. The transition between the gauge section and the full section was designed by an ellipse to minimize stress concentration. Following the tests, the gauge section of the fracture surface was measured for each specimen to derive the nominal stress. The LCF strength was studied in total strain-controlled fatigue tests, at an  $R$ -ratio of  $R_c = -1$  and total strain amplitudes in the range of  $0.22\% \leq \epsilon_a \leq 0.30\%$ . The frequency of the tests varied in the range of  $0.1 \text{ Hz} \leq f \leq 1 \text{ Hz}$ , depending on the strain level. As a failure criterion, a drop in tensile stress of 10% compared to the stabilized condition was used and defined as cycles to crack initiation.

To reveal the impact of heat treatment on the microstructure and mechanical properties of the Al-13Mg-1.1Zn-0.9Cu-0.6Si CCA, homogenization annealing was carried out at 460 and 465 °C for 3, 6, and 24 h. All specimens were water-quenched after homogenization.

### 3. Results

#### 3.1. Microstructure

The microstructure of the Al-13Mg-1.1Zn-0.9Cu-0.6Si CCA was studied via OM and SEM, as displayed in **Figure 1**. As can be

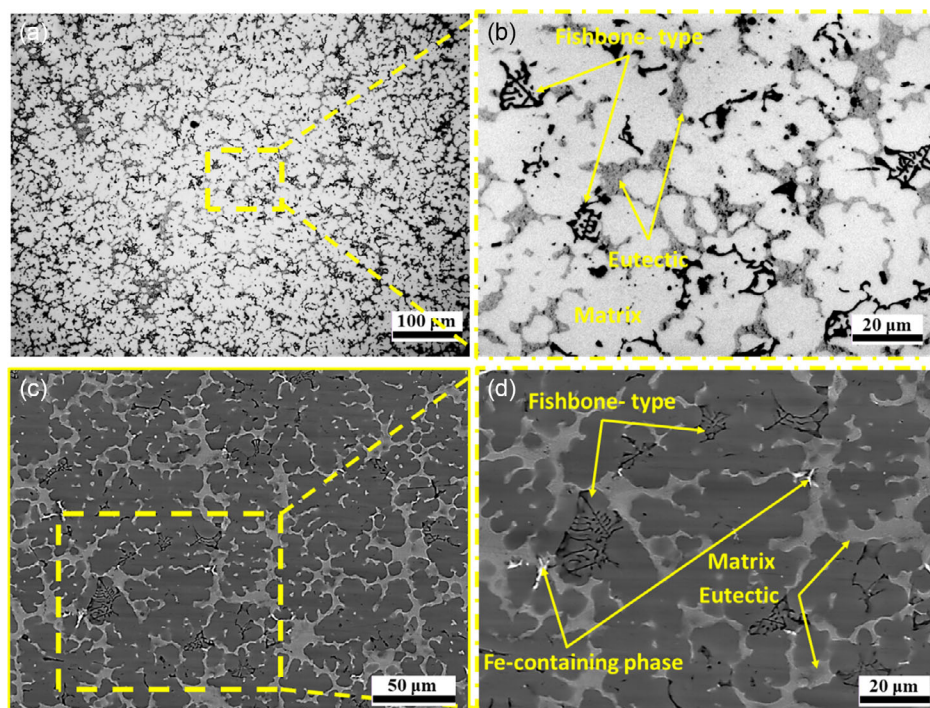


**Figure 1.** a,b) Optical micrographs; c,d) BSE images of Al-13Mg-1.1Zn-0.9Cu-0.6Si CCA. Details of respective optical micrographs and BSE images at higher magnification are shown and marked with yellow dashed rectangles. Microstructural features are marked by arrows. The microstructure of this CCA is composed of various phases, namely the Al-matrix, eutectic, and fishbone-type structures.

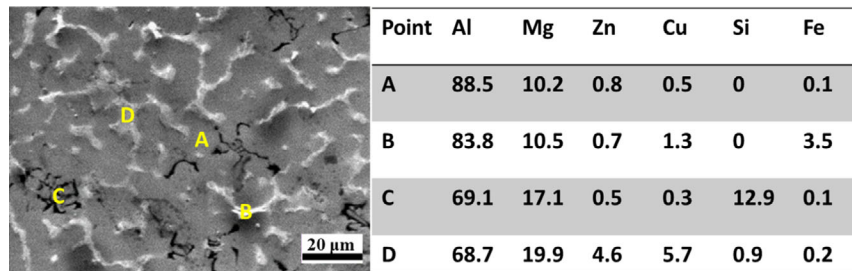


**Figure 2.** SEM micrograph of the Al-13Mg-1.1Zn-0.9Cu-0.6Si CCA using SE mode. Chemical compositions (at%) of phases marked in the microstructure are summarized in the table. Points A, B, C, and D are related to the matrix, an Fe-containing precipitate, the fishbone-type structure, and the eutectic structure, respectively.

seen, the microstructure of this CCA consists of different phases. Eutectic and fishbone-type structures are embedded in the Al-matrix. In a previous study on Al-11.5Mg-2.6Zn-2.1Cu-0.6Si CCA, both eutectic and fishbone-type structures were also observed.<sup>[21]</sup> It is well-known that intermetallic phases in Al alloys can form fishbone-type microstructure or “Chinese-Script” morphology,<sup>[31–33]</sup> e.g., the Mg<sub>2</sub>Si phase.<sup>[34]</sup> Various phases in the microstructure of this CCA have different effects on its mechanical properties. Solidification of the CCA was simulated via JMatPro. First, an  $\alpha$ -aluminum solid solution forms around 600 °C. Next, Fe-containing phases and Mg<sub>2</sub>Si precipitate from the melt. Around 480 °C, a final eutectic solidification to  $\alpha$  + AlZnMgCu-phases takes place.

The chemical compositions of the different phases in the Al-13Mg-1.1Zn-0.9Cu-0.6Si CCA are determined by EDS analysis. The chemical compositions of the phases are summarized in **Figure 2**. Considering JMatPro simulation and EDS analysis, the matrix (point A) has high Al content, while it has very low Zn, Si, and Fe contents. It represents the  $\alpha$ -aluminum solid solution. The eutectic structure consists of  $\alpha$  + AlZnMgCu-phases (point D). A previous study on this kind of CCA also reported on the eutectic phase.<sup>[21]</sup> The eutectic structures were reported to be  $\alpha$ -Al + Mg<sub>32</sub>(AlZn)<sub>49</sub>. The bright particles (point B) have a higher Fe content compared to the matrix. These are primary Fe-containing precipitates. The fishbone-type structure (point C) is rich in Si and Mg. It belongs to the Mg<sub>2</sub>Si phase. Similar fishbone-type Mg<sub>2</sub>Si particles have been found in an AlMg<sub>9</sub> cast alloy.<sup>[34]</sup>

**Figure 3** displays the results obtained by ED-XRD of the Al-13Mg-1.1Zn-0.9Cu-0.6Si CCA. ED-XRD reveals that this CCA consists of different phases, namely face-centered cubic (FCC) and Mg<sub>32</sub>(AlZn)<sub>49</sub> phases. The FCC and Mg<sub>32</sub>(AlZn)<sub>49</sub> phases are supposed to be the  $\alpha$ -Al-matrix and the eutectic phase, respectively. The ED-XRD results elaborated in the present study are in agreement with the results reported in the study of Shao et al.<sup>[21]</sup>

### 3.2. Mechanical Properties under Monotonic Loading

The hardness of the Al-13Mg-1.1Zn-0.9Cu-0.6Si CCA was found to be 120.4 ± 4.3 HV 0.5. Clearly, the hardness value cannot resolve the hardness of each phase present in the microstructure. To characterize the mechanical properties of each phase and estimate their hardness values, nanoindentation measurements were carried out, as demonstrated in **Figure 4**. It should

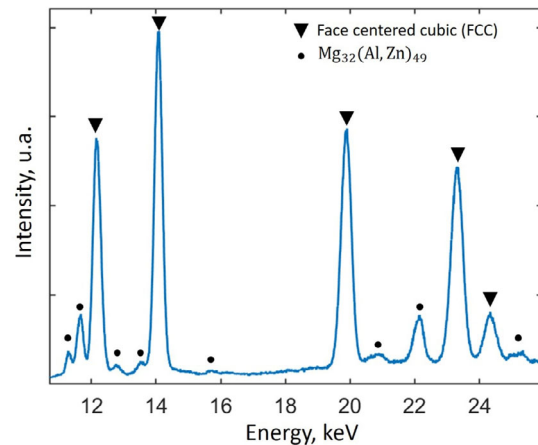


**Figure 3.** Energy-dispersive X-ray diffraction pattern of the Al-13Mg-1.1Zn-0.9Cu-0.6Si CCA; FCC and Mg<sub>32</sub>(AlZn)<sub>49</sub> were identified. The X-ray diffraction pattern clearly reveals that this CCA consists of different phases.

be noted that although matrix and eutectic phases were successfully characterized, the fishbone-type structure could not be reliably analyzed using the setup employed. The nanoindentation data attained for the fishbone-type structure showed a considerable scatter, which could be related to the fine and narrow features of this phase. Nanoindentation results reveal that the penetration depth (Pd) is substantially lower (120 nm) in the eutectic region compared to that of the Pd in the matrix (162 nm). The estimated hardness values of the matrix and eutectic phases are 160 Vickers instrumented hardness (HVIT) and 336 HVIT, respectively. It was previously reported that the eutectic structure in an Al-Cu-Si cast alloy has a significantly higher hardness in comparison to the matrix,<sup>[35]</sup> i.e., due to the higher content of the alloying elements and its morphology, respectively, the eutectic phase is supposed to be harder than the Al-matrix.

The monotonic mechanical properties of the Al-13Mg-1.1Zn-0.9Cu-0.6Si CCA were studied under tension and compression. Results are shown in **Figure 5**. Obviously, the CCA exhibits very different characteristics under tension and compression. In general, this alloy shows a very brittle behavior upon tensile loading. The ultimate tensile strength (UTS) and fracture strain (A) were 185.4 ± 23.6 MPa and 0.8 ± 0.3%, respectively. Under compressive loading, the ultimate compressive strength (UCS) and

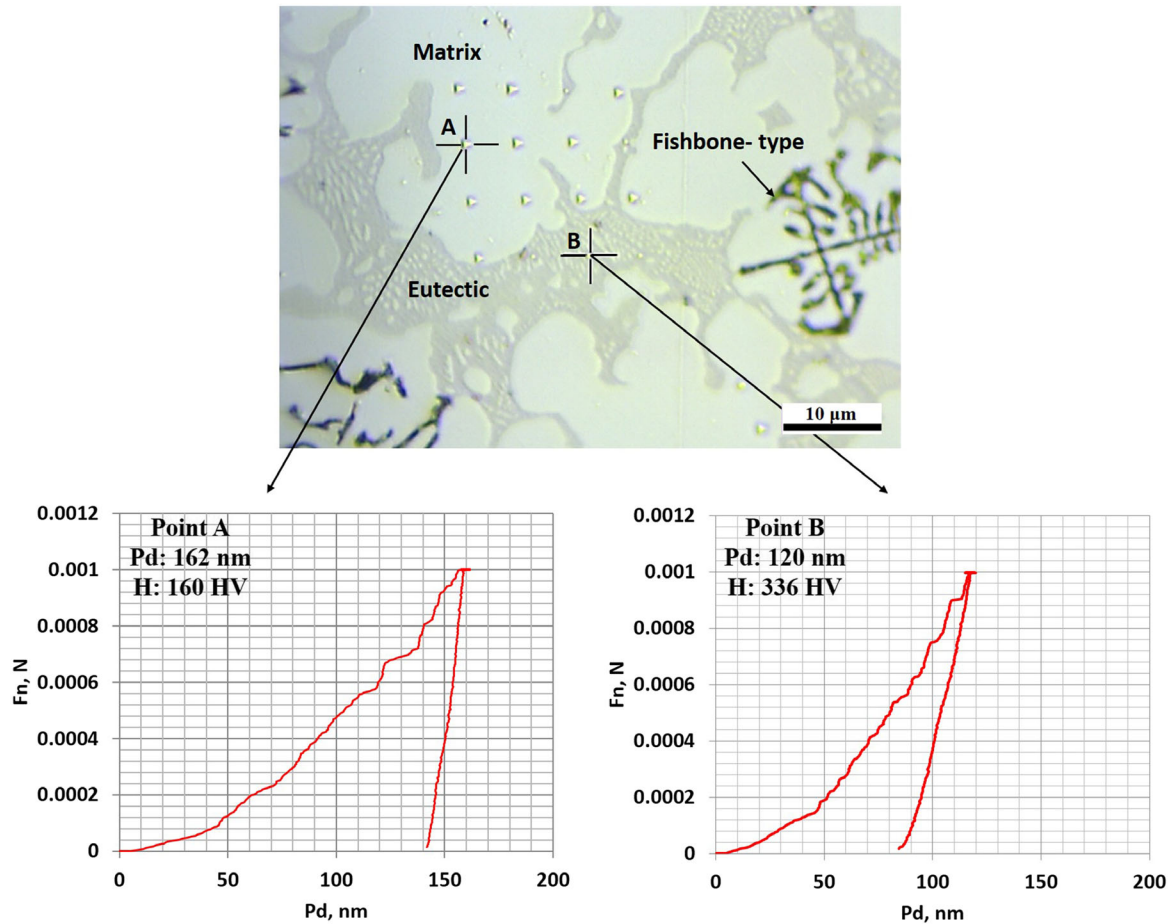
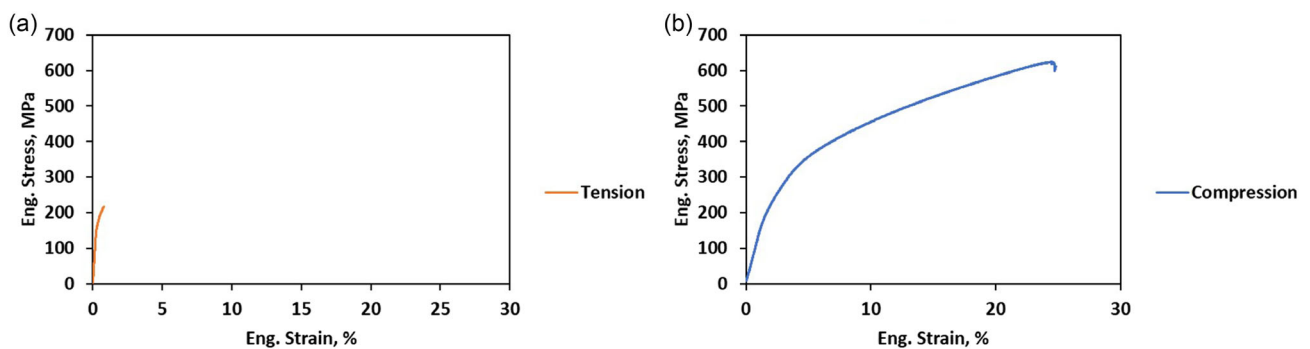


**Figure 4.** Nanoindentation measurements performed at various points. Penetration depths (Pd) for the matrix and the eutectic phase versus indentation loads are plotted. The penetration depth (Pd) is considerably lower (120 nm) in the eutectic region in comparison to the Pd in the matrix (162 nm).



Loading Condition	UTS/UCS, MPa	Fracture Strain, %
Tension	185.4 ± 23.6	0.8 ± 0.3
Compression	605.4 ± 17.7	23.0 ± 1.9

**Figure 5.** a) Tensile and b) compressive stress–strain curve of the Al-13Mg-1.1Zn-0.9Cu-0.6Si CCA; although this CCA shows relatively good mechanical properties under compressive loading, very poor tensile properties were observed. The table to the bottom lists the characteristic values including standard deviations.

fracture strain were  $605.4 \pm 17.7$  MPa and  $23.0 \pm 1.9\%$ , respectively. Poor tensile properties and brittle behavior observed under tensile loading can be ascribed to the formation of the brittle and detrimental fishbone-type intermetallic phases. It is well-documented that intermetallic phases with sharp edges can result in premature fracture in as-cast Al alloys.<sup>[36,37]</sup> Besides, debonding of Si-rich particles was also mentioned to cause brittle behavior.<sup>[36]</sup>

### 3.3. Mechanical Properties under Cyclic Loading

The  $\epsilon$ -N curve of the Al-13Mg-1.1Zn-0.9Cu-0.6Si CCA in the LCF regime was determined with six specimens at an  $R_\epsilon = -1$  tested at room temperature, **Figure 6**. Assessment of the strain-controlled fatigue tests reveals only a quite low amount of plastic strain even at the highest strain amplitude of  $\epsilon_a = 0.30\%$ . With a fatigue strength exponent  $b = -0.0195$ , the slope is comparatively shallow. The values of typical wrought and cast aluminum alloys are in the range of  $b = -0.17$  to  $-0.04$  according to Fatemi et al.<sup>[38]</sup> and Ostermann.<sup>[39]</sup>

The cyclic stress-strain curve being derived by considering compatibility between the parameters of the  $\epsilon$ -N curve and the parameters  $K'$  and  $n'$  shows slight hardening compared to the initial stress-strain curve, **Figure 7**.

The fracture surfaces of all specimens were analyzed by SEM, **Figure 8**. The exact location of crack initiation could not be located; however, various areas featuring pronounced shrinkage porosity were identified. It is likely that failure starts from these locations and propagates further into the material. No distinction could be made on the fracture surface between regions of stable crack-propagation and brittle fracture.

The quite low endurable strains in the strain-controlled fatigue tests can likely be linked to the identified shrinkage porosity. This porosity leads to local stress concentrations and eventually to lower fatigue life. This behavior is known from other cast materials, such as ductile cast iron and AlSi10Mg.<sup>[40,41]</sup>

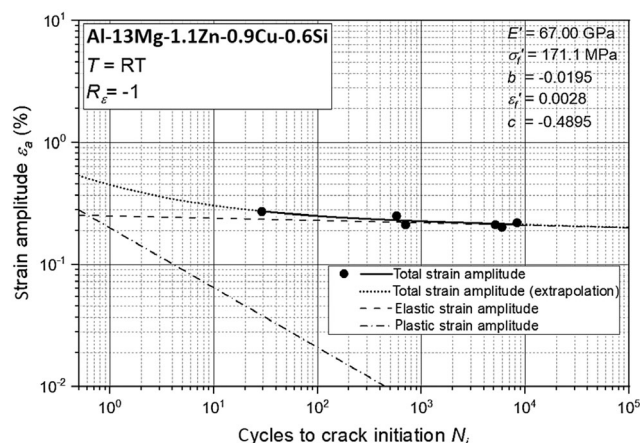


**Figure 6.**  $\epsilon$ -N curve of the Al-13Mg-1.1Zn-0.9Cu-0.6Si CCA in the LCF regime; a minor contribution of plastic strain even at the highest strain amplitude was observed.

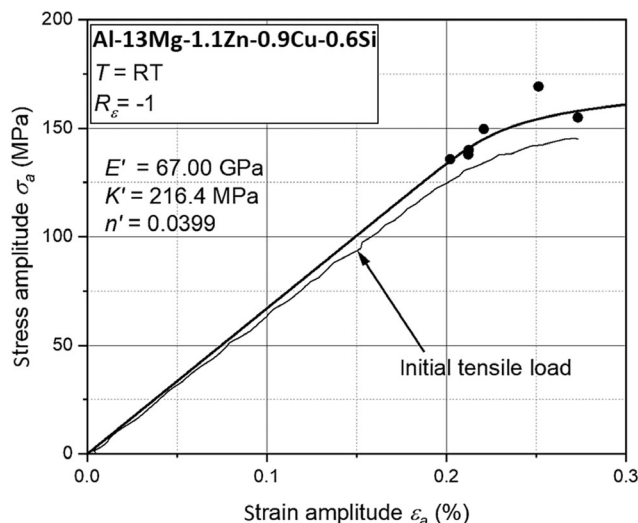


**Figure 7.** Cyclic stress-strain curve of the Al-13Mg-1.1Zn-0.9Cu-0.6Si CCA; the parameters  $K'$  and  $n'$  points at a gradual hardening in comparison to the initial stress-strain curve.

### 3.4. DSC Analysis and Heat Treatment

Homogenization annealing is a common heat treatment to spheroidize primary precipitates in cast aluminum alloys and thereby improve their mechanical properties. It is typically performed slightly below the melting start temperature. The DSC curve in **Figure 9** shows the melting behavior of the CCA in focus. A sharp melting peak starts around  $480^\circ\text{C}$  and indicates eutectic melting. Further melting consists of several overlapping reactions and finishes around  $600^\circ\text{C}$ . This result agrees with the above-mentioned JMatPro simulation.

In light of the DSC measurements, homogenization at  $460^\circ\text{C}$  and  $465^\circ\text{C}$  has been selected for the Al-13Mg-1.1Zn-0.9Cu-0.6Si CCA. At higher temperatures localized melting can take place. Optical micrographs of the specimens upon homogenization at  $460^\circ\text{C}$  and  $465^\circ\text{C}$  for 3, 6, and 24 h are shown in **Figure 10**. Homogenization of this CCA at both temperatures for longer soaking times resulted in the spheroidization of all coarse precipitates, also of the Chinese Script  $\text{Mg}_2\text{Si}$ .

As displayed in **Figure 11**, tensile experiments were carried out on the specimens homogenized at  $465^\circ\text{C}$  for different soaking times. Accordingly, homogenization could not improve the mechanical properties of the cast Al-13Mg-1.1Zn-0.9Cu-0.6Si CCA significantly. The brittle behavior and inferior mechanical properties even after homogenization are thought to stem from the presence of shrinkage porosity and/or coarse primary precipitates even after spheroidization. As no improvement of the tensile properties was seen, the homogenized specimens were not subjected to additional fatigue tests.

## 4. Discussion

### 4.1. Aspects of Microstructural Features

Different techniques showed that the microstructure of the Al-13Mg-1.1Zn-0.9Cu-0.6Si CCA consists of different phases,

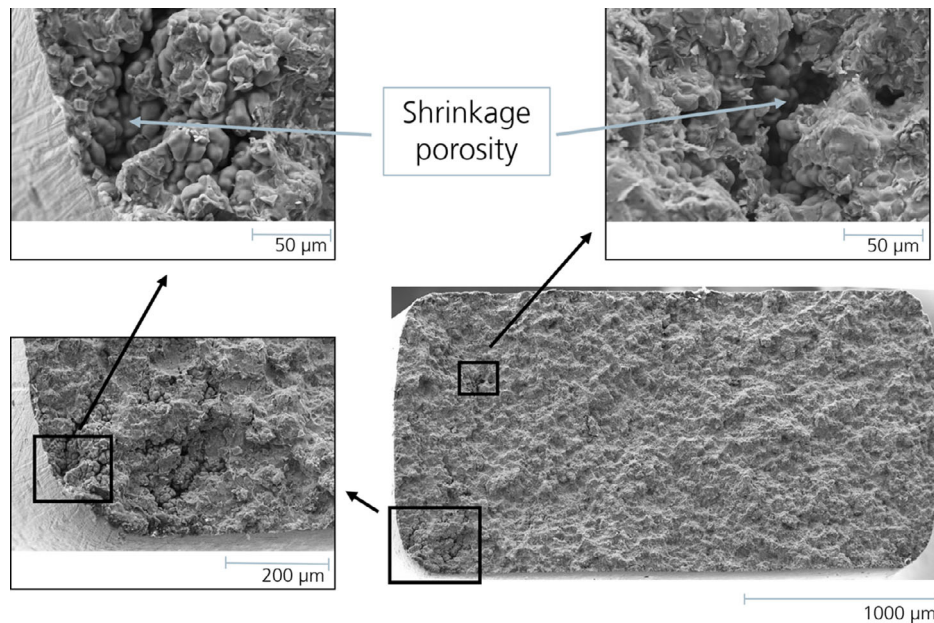


**Figure 8.** Fracture surface of the specimen failed at  $N_f = 576$  cycles at a strain amplitude of  $\epsilon_a = 0.25\%$ ; fatigue cracks are thought to be initiated from the shrinkage porosity observed.

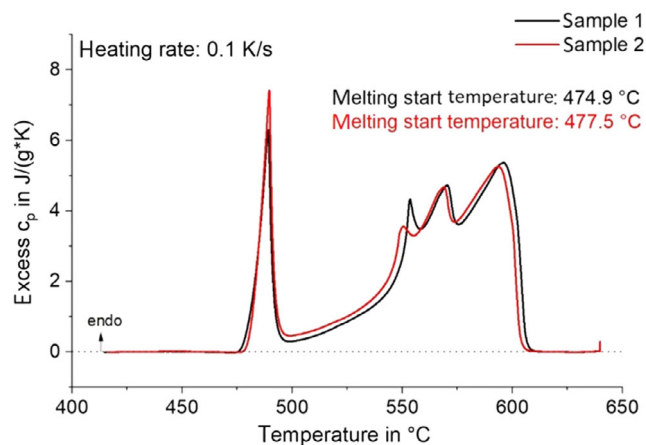


**Figure 9.** DSC melting experiments on the Al-13Mg-1.1Zn-0.9Cu-0.6Si CCA at a heating rate of  $0.1 \text{ K s}^{-1}$ ; The melting of the eutectic phase occurred at around  $480^\circ\text{C}$ . Further melting events include several overlapping reactions and end at around  $600^\circ\text{C}$ .

namely  $\alpha$ -Al-matrix, eutectic  $\alpha$ -Al +  $\text{Mg}_{32}(\text{AlZn})_{49}$ , Fe-containing phase, and Chinese Script  $\text{Mg}_2\text{Si}$  (see Figure 1–3). In the literature, the Chinese Script was documented for other cast Al alloys as well.<sup>[31–33]</sup> It was previously reported that an increase in Mg content can enhance the formation of the Chinese Script  $\text{Mg}_2\text{Si}$ .<sup>[42]</sup> Higher Mg content can promote precipitation of  $\text{Mg}_2\text{Si}$  particles via diffusion of Mg toward second-phase particles. During slow cooling of the alloy upon solidification, the flux of solute atoms toward already formed precipitates is promoted, causing the growth of the Chinese Script  $\text{Mg}_2\text{Si}$ . Another feature observed in the microstructure of this CCA is the eutectic phase. According to the previous study on low-density CCAs, the

eutectic structure in Al-11.5Mg-2.6Zn-2.1Cu-0.6Si CCA consists of  $\alpha$  +  $\text{Mg}_2\text{Si}$ -phases.<sup>[21]</sup> However, microstructural analysis and simulation via JMatPro in the present study indicate that the eutectic is composed of  $\alpha$  + AlZnMgCu-phases.

#### 4.2. Aspects of Mechanical Properties and Damage Mechanism

The different phases present in the Al-13Mg-1.1Zn-0.9Cu-0.6Si CCA have various impacts on the mechanical properties in different regimes. The presence of the Chinese Script  $\text{Mg}_2\text{Si}$  and shrinkage porosities in the as-cast Al-13Mg-1.1Zn-0.9Cu-0.6Si CCA cause adverse mechanical properties in both monotonic and cyclic loading regimes (see Figure 5 and 6). The results of the present study reveal that this alloy shows a very brittle behavior under tension. This can be attributed to the brittle essence of such intermetallic phases.<sup>[36,37]</sup> Besides, the formation of shrinkage porosity can detrimentally affect both tensile and fatigue performances. Shrinkage defects usually evolve when the melt is not able to feed the volume contraction in the solidification process.<sup>[43]</sup> Such defects make the alloy prone to crack nucleation upon monotonic and cyclic loading. The size and morphologies of these defects can highly affect the mechanical properties of the Al-13Mg-1.1Zn-0.9Cu-0.6Si CCA. In the present study, defects observed are relatively large (see Figure 8) and expected to be very detrimental to the mechanical properties of this CCA in both monotonic and cyclic regimes.

#### 4.3. Comparison between Al-13Mg-1.1Zn-0.9Cu-0.6Si CCA and Other Low-Density and Lightweight CCAs

Exploring the mechanical properties of low-density CCAs and comparing them with conventional CCAs and commercially

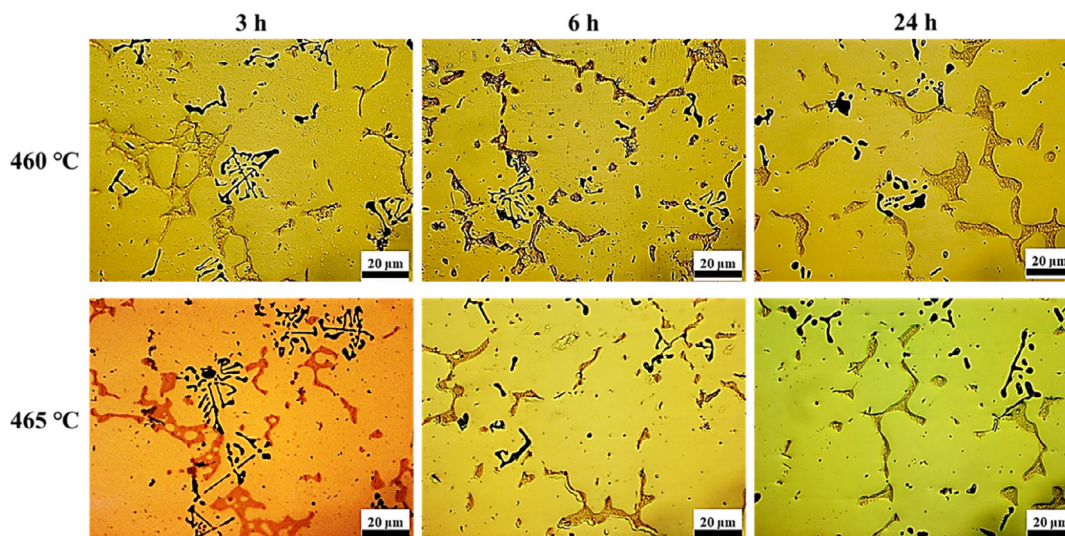


**Figure 10.** Optical micrographs of the specimens upon homogenization at 460 and 465 °C for 3, 6, and 24 h. The first and second rows show microstructures of specimens heat treated at 460 and 465 °C, respectively. The first, second, and third columns display specimens heat treated for 3, 6, and 24 h, respectively. Homogenization of this CCA at both temperatures for longer soaking durations led to the spheroidization of all coarse precipitates including the Chinese Script  $Mg_2Si$ .

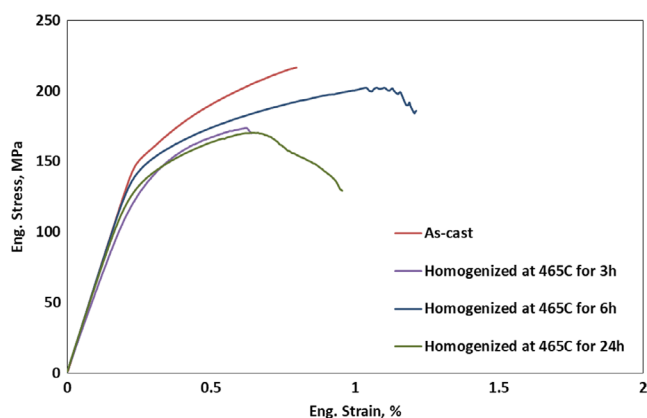


**Figure 11.** Tensile curves of homogenized specimens heat treated at 465 °C for different soaking times (3, 6, and 24 h). For the sake of direct comparison, the tensile curve of the as-cast specimen is also shown (see Figure 4a). Homogenization for various soaking durations could not improve tensile properties of the CCA in focus.

available engineering alloys were the focus of several studies in recent years.<sup>[21–29]</sup> The compressive mechanical properties of low-density CCAs are summarized in **Table 2**. It can be seen that with an increase in Al content, the YS and UCS values decreased in most cases, while the compressive plasticity has been enhanced. On the one hand, the reduction in the compressive strength of CCAs with an increase in Al content can be attributed to the increase in volume fraction of the soft  $\alpha$ -Al phase.<sup>[21]</sup> On the other hand, the increase in the fracture strain values for the CCAs with a higher Al content can be rationalized by the reduction in the volume fraction of intermetallic phases.<sup>[27]</sup> It is also

**Table 2.** Compressive mechanical properties of several low-density CCAs. The chemical compositions of CCAs are reported in at%.

Alloy	YS [MPa]	UCS [MPa]	A [%]	Ref.
$Al_{80}Mg_5Sn_5Zn_5Ni_5$	317	447	15	[27]
$Al_{80}Mg_5Sn_5Zn_5Mn_5$	336	368	14	[27]
$Al_{180}Mg_5Sn_5Zn_5Ti_5$	420	563	12	[27]
$Al_{19.9}Li_{30}Mg_{35}Si_{10}Ca_5Y_{0.1}$	556	710	2	[28]
$Al_{15}Li_{35}Mg_{35}Ca_{10}Si_5$	418	516	15	[28]
$Al_{15}Li_{38}Mg_{45}Ca_{0.5}Si_{1.5}$	342	445	45	[28]
$Al_{15}Li_{39}Mg_{45}Ca_{0.5}Si_{0.5}$	300	535	60	[28]
$Al_{15}Li_{35}Mg_{48}Ca_1Si_1$	360	596	10	[28]
$Al_{58.5}Mg_{31.5}Zn_{4.5}Cu_{4.5}Si_1$	–	577	3.2	[21]
$Al_{63}Mg_{27}Zn_{4.5}Cu_{4.5}Si_1$	–	679	1.9	[21]
$Al_{66.7}Mg_{23.3}Zn_{4.5}Cu_{4.5}Si_1$	–	660	4.2	[21]
$Al_{80}Mg_{14}Zn_{2.7}Cu_{2.7}Si_{0.6}$	203	498	13.8	[21]
$Al_{85}Mg_{10.5}Zn_{2.025}Cu_{2.025}Si_{0.45}$	255	814	24.8	[21]
$Al_{90}Mg_7Zn_{1.35}Cu_{1.35}Si_{0.3}$	198	794	32.7	[21]
Al-13Mg-1.1Zn-0.9Cu-0.6Si	223	605	23	Present Study

worth noting that adding a small amount of Ca and Y promotes strengthening of low-density CCAs. The mechanical properties of the Al-13Mg-1.1Zn-0.9Cu-0.6Si under compression are very good compared to other low-density CCAs since both relatively high UCS and fracture strain were obtained. Another point that should be taken into account is that, in comparison to other low-density CCAs, the Al-13Mg-1.1Zn-0.9Cu-0.6Si CCA exhibited a high ratio of YS/UCS pointing at its strain hardening capability under compressive loading.



Although the tensile properties of the Al-13Mg-1.1Zn-0.9Cu-0.6Si CCA were characterized in the present study, the lack of data for other low-density CCAs does not allow a comparative study of the results obtained. Therefore, to assess the mechanical properties of the CCA in focus of the present study, its tensile properties are compared with some of the lightweight CCAs, as summarized in **Table 3**. The tensile properties of the Al-13Mg-1.1Zn-0.9Cu-0.6Si CCA are inferior compared to those of the lightweight CCAs. Tensile properties of  $Zr_{1.2}V_{0.8}NbTi_xAl_y$  CCAs are superior as in this case the formation of the B2 and C14 Laves precipitates were suppressed resulting in a single body-centered-cubic (BCC) phase structure.<sup>[20]</sup> The tensile properties of  $Ti_{70}Al_{15}V_{15}$  and  $Ti_{80}Al_{10}V_{10}$  lightweight CCA were reported elsewhere.<sup>[44]</sup> It was mentioned that  $Ti_{70}Al_{15}V_{15}$  consisted of a BCC structure with a small amount of B2 phase, while  $Ti_{80}Al_{10}V_{10}$  had a BCC/hexagon close-packed (HCP) dual-phase structure.  $Ti_{80}Al_{10}V_{10}$  had a higher interface density in comparison with  $Ti_{70}Al_{15}V_{15}$ , eventually promoting significant work hardening in this CCA. The poor tensile properties of the Al-13Mg-1.1Zn-0.9Cu-0.6Si CCA compared to the listed lightweight CCAs are thought to be induced by the formation of brittle and undesired intermetallic phases.

#### 4.4. Outlook and Future Research

Although homogenization could not enhance the mechanical properties of the CCA in focus, by appropriate thermomechanical treatments one might expect the poor tensile and fatigue properties to be improved. Thermomechanical treatments can alter the microstructure of this CCA and eventually affect the mechanical properties in both monotonic and cyclic regimes. Previous studies<sup>[45–50]</sup> on Al alloys showed great potential for the improvement of mechanical properties by the employment of thermo-mechanical treatments. Besides, the casting process parameters prevailing during solidification have a significant influence on densification and eventually mechanical properties of this kind of CCA.<sup>[43]</sup> Therefore, the assessment of casting parameters opens up pathways toward the enhancement of component quality and mechanical properties. The potential for improvement has not been investigated in the present study since it is beyond the scope of current research work. However, the effect of various thermomechanical treatments should be addressed in future research.

**Table 3.** Tensile properties of lightweight CCAs in comparison to the Al-13Mg-1.1Zn-0.9Cu-0.6Si CCA. The chemical compositions of CCAs are given in at%.

Alloy	YS [MPa]	UTS [MPa]	A [%]	Ref.
$Zr_{1.2}V_{0.8}NbTi_2Al_{0.3}$	1,100	≈1,300	>37	[20]
$Zr_{1.2}V_{0.8}NbTi_{3.6}Al_{0.3}$	850	≈1,100	>30	[20]
$Zr_{1.2}V_{0.8}NbTi_{3.6}Al_{0.6}$	1,000	≈1,175	>30	[20]
$Ti_{70}Al_{15}V_{15}$	556	≈590	13	[44]
$Ti_{80}Al_{10}V_{10}$	657	≈900	10	[44]
Al-13Mg-1.1Zn-0.9Cu-0.6Si	158	185	0.8	Present Study

## 5. Conclusion

The monotonic and cyclic behavior of an Al-13Mg-1.1Zn-0.9Cu-0.6Si CCA was studied. According to the results obtained, the following conclusions can be made: 1) Four microstructure constituents, i.e., an  $\alpha$ -Al-matrix, a eutectic structure composed of  $\alpha + AlZnMgCu$  phase, a primary Fe-containing phase, and fishbone-type  $Mg_2Si$ , were detected in the as-cast condition of the Al-13Mg-1.1Zn-0.9Cu-0.6Si CCA. Energy-dispersive X-ray diffraction measurements revealed that this CCA consists of face-centered cubic (FCC) and  $Mg_{32}(AlZn)_{49}$  phases. 2) Nanoindentation measurements revealed that the matrix has lower hardness compared to the eutectic microstructure. Considering tensile testing, the ultimate tensile strength and fracture strain were measured to be  $185.4 \pm 23.6$  MPa and  $0.8 \pm 0.3\%$ , respectively. In compression testing, the ultimate compressive strength and fracture strain were measured to be  $605.4 \pm 17.7$  MPa and  $23.0 \pm 1.9\%$ , respectively. 3) Evaluation of the strain-controlled fatigue experiments revealed that even at the highest strain amplitude of  $\epsilon_a = 0.30\%$ , only very limited plastic strain occurs. The cyclic stress–strain curve exhibited a slight hardening in comparison to the initial stress–strain curve. 4) Microstructural studies and fracture analysis clearly revealed that the presence of intermetallic brittle phases and shrinkage defects are the main reason for the poor tensile properties and fatigue performance of the Al-13Mg-1.1Zn-0.9Cu-0.6Si CCA 5) Homogenization at 460 and 465 °C for 3, 6, and 24 h led to the spheroidization of all primary precipitates, also of the Chinese Script  $Mg_2Si$ . However, the homogenization could not improve the mechanical properties of this CCA significantly.

## Acknowledgements

The authors of this research article would like to express deep gratitude to the project ALLEGRO funded by the Hessen State Ministry for Higher Education, Research and the Arts-Initiative for the Development of Scientific and Economic Excellence (LOEWE). The authors would like to thank Mr. Artjom Bolender for conducting the ED-XRD measurement.

Open Access funding enabled and organized by Projekt DEAL.

## Conflict of Interest

The authors declare no conflict of interest.

## Author Contributions

S.V.S., J.B., and T.N.: Conceptualization; S.V.S., J.B., M.K., A.M., M.G., H.F., and M.R.: Data curation; S.V.S., J.B., M.K., A.M., M.G., H.F., and M.R.: Formal analysis; M.F., O.K., S.B., M.O. T.M., and T.N.: Funding acquisition; S.V.S., J.B., M.K., A.M., M.G., H.F., M.K., and M.R.: Investigation; S.V.S.: Methodology; M.F., O.K., S.B., M.O. T.M., and T.N.: Project administration; M.F., O.K., S.B., M.O. T.M., and T.N.: Resources; S M.F., O.K., S.B., M.O. T.M., and T.N.: Supervision; S.V.S. and J.B.: Visualization; S.V.S. and J.B.: Writing—original draft; S.V.S., J.B., H.F., M.K., A.M., M.K.I., M.R., M.F., O.K., S.B., M.O. T.M., and T.N.: Writing—review & editing. All authors have read and agreed to the published version of the manuscript.

## Data Availability Statement

The data that support the findings of this study are available from the corresponding author upon reasonable request.

## Keywords

Al alloys, compositionally complex alloy, cyclic behavior, fatigue performance, microstructure, monotonic behavior

Received: June 12, 2023

Revised: July 31, 2023

Published online: August 18, 2023

- 
- [1] J. W. Yeh, S. K. Chen, S. J. Lin, J. Y. Gan, T. S. Chin, T. T. Shun, C. H. Tsau, S. Y. Chang, *Adv. Eng. Mater.* **2004**, *6*, 299.
- [2] B. Cantor, I. T. H. Chang, P. Knight, A. J. B. Vincent, *Mater. Sci. Eng. A* **2004**, *375–377*, 213.
- [3] S. Picak, T. Wegener, S. V. Sajadifar, C. Sobrero, J. Richter, H. Kim, T. Niendorf, I. Karaman, *Acta Mater.* **2021**, *205*, 116540.
- [4] E. P. George, D. Raabe, R. O. Ritchie, *Nat. Rev. Mater.* **2019**, *4*, 515.
- [5] Z. Li, K. G. Pradeep, Y. Deng, D. Raabe, C. C. Tasan, *Nature* **2016**, *534*, 227.
- [6] P. K. Huang, J. W. Yeh, T. T. Shun, S. K. Chen, *Adv. Eng. Mater.* **2004**, *6*, 74.
- [7] M. H. Asoushe, A. Z. Hanzaki, H. R. Abedi, B. Mirshekari, T. Wegener, S. V. Sajadifar, T. Niendorf, *Mater. Sci. Eng. A* **2021**, *799*, 140012.
- [8] H. Inui, K. Kishida, L. Li, A. M. Manzoni, S. Haas, U. Glatzel, *MRS Bull.* **2022**, *47*, 168.
- [9] A. M. Hossain, N. Kumar, *J. Alloys Compd.* **2022**, *893*, 162152.
- [10] Z. Li, D. Raabe, *JOM* **2017**, *69*, 2099.
- [11] A. Gesing, R. Wolanski, *JOM* **2001**, *53*, 21.
- [12] C. H. Cáceres, *Mater. Des.* **2009**, *30*, 2813.
- [13] M. Tisza, I. Czinege, *Int. J. Light. Mater. Manuf.* **2018**, *1*, 229.
- [14] S. V. Sajadifar, T. Suckow, C. K. Chandra, B. Heider, A. Heidarzadeh, J. Zavašnik, R. Reitz, M. Oechsner, P. Groche, T. Niendorf, *J. Manuf. Process.* **2023**, *86*, 336.
- [15] Y. Xu, Z. Zhang, Z. Gao, Y. Bai, P. Zhao, W. Mao, *Mater. Charact.* **2021**, *182*, 111559.
- [16] E. Georgantzia, M. Gkantou, G. S. Kamaris, *Eng. Struct.* **2021**, *227*, 111372.
- [17] Y. Li, Z. R. Zhang, Z. Y. Zhao, H. X. Li, L. Katgerman, J. S. Zhang, L. Z. Zhuang, *Metall. Mater. Trans. A Phys. Metall. Mater. Sci.* **2019**, *50*, 3603.
- [18] Y. Liu, Z. Zhu, Z. Wang, B. Zhu, Y. Wang, Y. Zhang, *Proc. Eng.* **2017**, *207*, 723.
- [19] K. Senthil, M. A. Iqbal, P. S. Chandel, N. Gupta, *Int. J. Impact Eng.* **2017**, *108*, 171.
- [20] L. Wang, S. Chen, B. Li, T. Cao, B. Wang, L. Wang, Y. Ren, J. Liang, Y. Xue, *Mater. Sci. Eng. A* **2021**, *814*, 141234.
- [21] L. Shao, T. Zhang, L. Li, Y. Zhao, J. Huang, P. K. Liaw, Y. Zhang, *J. Mater. Eng. Perform.* **2018**, *27*, 6648.
- [22] R. Feng, M. C. Gao, C. Zhang, W. Guo, J. D. Poplawsky, F. Zhang, J. A. Hawk, J. C. Neuefeind, Y. Ren, P. K. Liaw, *Acta Mater.* **2018**, *146*, 280.
- [23] R. Feng, C. Zhang, M. C. Gao, Z. Pei, F. Zhang, Y. Chen, D. Ma, K. An, J. D. Poplawsky, L. Ouyang, Y. Ren, J. A. Hawk, M. Widom, P. K. Liaw, *Nat. Commun.* **2021**, *12*, 4329.
- [24] S. Gorsse, D. B. Miracle, O. N. Senkov, *Acta Mater.* **2017**, *135*, 177.
- [25] D. B. Miracle, O. N. Senkov, *Acta Mater.* **2017**, *122*, 448.
- [26] J. M. Sanchez, I. Vicario, J. Albizuri, T. Guraya, J. C. Garcia, *J. Mater. Res. Technol.* **2019**, *8*, 795.
- [27] J. M. Sanchez, A. Pascual, I. Vicario, J. Albizuri, T. Guraya, H. Galarraga, *Metals* **2021**, *11*, 1944.
- [28] Y. Jia, Y. Jia, S. Wu, X. Ma, G. Wang, *Mater.* **2019**, *12*, 1136.
- [29] X. Yang, S. Y. Chen, J. D. Cotton, Y. Zhang, *JOM* **2014**, *66*, 2009.
- [30] H. Fröck, M. Reich, B. Milkereit, O. Kessler, *Materials* **2019**, *12*, 1085.
- [31] R. Kakitani, A. Garcia, N. Cheung, *Adv. Eng. Mater.* **2020**, *22*, 2000503.
- [32] H. L. De Moraes, J. R. De Oliveira, D. C. R. Espinosa, J. A. S. Tenório, *Mater. Trans.* **2006**, *47*, 1731.
- [33] A. M. A. Mohamed, E. Samuel, Y. Zedan, A. M. Samuel, H. W. Doty, F. H. Samuel, *Mater.* **2022**, *15*, 1335.
- [34] P. Snopiński, M. Król, T. Tański, B. Krupińska, *J. Therm. Anal. Calorim.* **2018**, *133*, 379.
- [35] S. L. dos Santos, F. R. Toloczko, A. C. Merij, N. H. Saito, D. M. da Silva, *Mater. Res.* **2021**, *24*, 20200329.
- [36] M. Tiryakioğlu, *Mater.* **2020**, *13*, 2019.
- [37] L. Kuchariková, D. Medvecká, E. Tillová, J. Belan, M. Kritikos, M. Chalupová, M. Uhrčík, *Mater.* **2021**, *14*, 1943.
- [38] A. Fatemi, A. Plaseied, A. K. Khosrovaneh, D. Tanner, *Int. J. Fatigue* **2005**, *27*, 1040.
- [39] F. Ostermann, in *Anwendungstechnologie Aluminium*, Springer Vieweg, Berlin, Heidelberg **2014**.
- [40] M. Krochmal, A. N. R. Rajan, G. Moieni, S. V. Sajadifar, T. Wegener, T. Niendorf, *J. Mater. Res.* **2022**, *38*, 297.
- [41] C. Bleicher, R. Wagener, H. Kaufmann, T. Melz, *SAE Int. J. Engines* **2017**, *10*, 340.
- [42] A. M. Samuel, Y. Zedan, E. A. Elsharkawi, M. H. Abdelaziz, F. H. Samuel, *Mater.* **2022**, *15*, 8844.
- [43] V. Khalajzadeh, C. Beckermann, *Metall. Mater. Trans. A Phys. Metall. Mater. Sci.* **2020**, *51*, 2239.
- [44] G. Lin, R. Guo, X. Shi, L. Han, J. Qiao, *Entropy* **2022**, *24*, 1777.
- [45] W. Ma, B. Wang, J. Lin, X. Tang, *Trans. Nonferrous Met. Soc. China* **2017**, *27*, 2454.
- [46] M. Maikranz-Valentin, U. Weidig, U. Schoof, H.-H. Becker, K. Steinhoff, *Steel Res. Int.* **2008**, *79*, 92.
- [47] S. V. Sajadifar, E. Scharifi, U. Weidig, K. Steinhoff, T. Niendorf, *HTM J. Heat Treat. Mater.* **2020**, *75*, 177.
- [48] S. V. Sajadifar, E. Scharifi, U. Weidig, K. Steinhoff, T. Niendorf, *Metals* **2020**, *10*, 884.
- [49] K. Shojaei, S. V. Sajadifar, G. G. Yapici, *Mater. Sci. Eng. A* **2016**, *670*, 81.
- [50] E. Scharifi, R. Knoth, U. Weidig, *Proc. Manuf.* **2019**, *29*, 481.